# Exploration of Inorganic Synthesis and Characterization of UiO-66-g-PEGMA Composite Membrane for Optimized Oil/Water Emulsion Separation Performance

Shangkum Yildun Goji[1]; Godwin Mafuyai[2]; Museyilnen Gocheka Mudel[1]; Jacob Shimwan Toekwal[3]; Rabiat Lawal Abdullahi[1]; Yusuf Garba Ranga[1]; John Stephen Gushit[4]

[1]Department of Chemistry, Faculty of Natural Sciences, P.M.B 2084, University of Jos, Nigeria

[2]Department of Chemistry, Faculty of Science, Plateau State University of Bokkos

[3]Department of Science Laboratory Technology, Plateau State Polytechnic Barkin Ladi P.M.B 2021, Plateau State

[4]Department of Science Laboratory Technology, Faculty of Natural Sciences, P.M.B 2084, University of Jos, Nigeria

**Corresponding Author**: gojis@unijos.edu.ng; Tel: +2348064562780

## Abstract

*Global challenge of separating emulsified oil/water mixtures is underscored by the extensive production of oily wastewater in industrial operations. Therefore, this study was focused on the exploration of inorganic synthesis and characterization of UiO-66-g-PEGMA composite membranes for optimized oil/water emulsion separation performance. Pristine UiO-66-$NH_2$ and UiO-66-g-PEGMA composite membranes were fabricated through vacuum suction filtration. The membranes, dispersed in deionized water through sonication, were deposited onto a cellulose nitrate (CN) substrate membrane under a constant differential pressure. The prepared membranes were characterized using various techniques, including ATR-IR, XRD, TEM, SEM, and TGA. Oil/water emulsion for evaluating membrane separation performance was prepared by stirring Ulvac oil R-2 in water with sodium dodecyl sulfate as a surfactant. Dynamic light scattering determined the droplet size distribution of the emulsion. The separation performance of composite membranes was assessed based on oil rejection, flux, and antifouling properties. Total flux decline (TR) and flux recovery ratio (FRR) were calculated to evaluate fouling resistance. The results indicated successful synthesis and grafting of UiO-66-g-PEGMA, with retained crystalline structure confirmed by XRD. The composite membrane exhibited enhanced fouling resistance and rejection compared to pristine UiO-66-$NH_2$. The introduction of grafted PEGMA improved hydrophilicity and partially filled interparticle voids, contributing to the enhanced filtration performance. The UiO-66-g-PEGMA membrane demonstrated improved water flux and antifouling capabilities without compromising oil retention. This study highlights the promising potential of UiO-66-g-PEGMA composite membranes in the design of high-performance membranes for effective oil/water separation. The research provides valuable insights into the application of inorganic synthesis techniques in addressing challenges associated with emulsion separation in oil-water separation processes.*

**Keywords:** UiO-66-g-PEGMA, Composite membranes, Oil/water emulsion separation, Characterization techniques, Fouling resistance, Inorganic synthesis techniques

# Exploration de la synthèse inorganique et caractérisation de la membrane composite UIO-66-G-PEGMA pour les performances de séparation des émulsions d'huile / eau optimisées


## Résumé

*Le défi mondial de séparer les mélanges d'huile / eau émulsifiés est souligné par la production approfondie des eaux usées huileuses dans les opérations industrielles. Par conséquent, cette étude a été axée sur l'exploration de la synthèse inorganique et la caractérisation des membranes composites UIO-66-G-PEGMA pour les performances optimisées de séparation des émulsions d'huile / eau. Les membranes composites UIO-66-NH2 et UIO-66-G-PEGMA ont été fabriquées par filtration d'aspiration sous vide. Les membranes, dispersées dans de l'eau désionisée par sonication, ont été déposées sur une membrane de substrat de nitrate de cellulose (NC) sous une pression différentielle constante. Les membranes préparées ont été caractérisées en utilisant diverses techniques, notamment ATR-IR, XRD, TEM, SEM et TGA. L'émulsion d'huile / eau pour évaluer les performances de séparation des membranes a été préparée en remuant l'huile ULVAC R-2 dans l'eau avec du dodécyl sulfate de sodium comme tensioactif. La diffusion dynamique de la lumière a déterminé la distribution de la taille des gouttelettes de l'émulsion. Les performances de séparation des membranes composites ont été évaluées sur la base du rejet d'huile, du flux et des propriétés antisfouling. La baisse du flux total (TR) et le rapport de récupération du flux (RRF) ont été calculées pour évaluer la résistance à l'encrassement. Les résultats ont indiqué une synthèse et une greffe réussies de l'UIO-66-G-PEGMA, avec une structure cristalline conservée confirmée par XRD. La membrane composite a montré une résistance et un rejet d'encrassement améliorés par rapport à UIO-66-NH2 vierge. L'introduction de la PEGMA greffée a amélioré l'hydrophilie et des vides interparticules partiellement remplis, contribuant aux performances de filtration améliorées. La membrane UIO-66-G-PEGMA a démontré une amélioration du flux d'eau et des capacités antifouling sans compromettre la rétention du pétrole. Cette étude met en évidence le potentiel prometteur des membranes composites UIO-66-G-PEGMA dans la conception de membranes haute performance pour une séparation efficace de l'huile / de l'eau. La recherche fournit des informations précieuses sur l'application des techniques de synthèse inorganiques pour relever les défis associés à la séparation des émulsions dans les processus de séparation des eaux pétroliers.*


**Mots-clés**: UIO-66-G-PEGMA, membranes composites, séparation d'émulsion à l'huile / eau, techniques de caractérisation, résistance à l'encrassement, techniques de synthèse inorganiques

ويؤكد التحدي العالمي المتمثل في فصل مخاليط الزيت المستحلب/الماء على نطاق واسع إنتاج مياه الصرف الصحي الزيتية في العمليات الصناعية لذلك، للأداء الأمثل لفصل UiO-66-g-PEGMA ركزت هذه الدراسة على استكشاف التوليف غير العضوي وتوصيف الأغشية المركبة تم تصنيعها من خلال ترشيح شفط الفراغالأغشية، UiO-66-g-PEGMA البكر والأغشية المركبة UiO-66-NH2 الزيت/مستحلب الماء

Shangkum Yildun Goji1; Godwin Mafuyai2; Museyilnen Gocheka Mudel1; Jacob Shimwan Toekwal3; Rabiat Lawal Abdullahi1; Yusuf Garba Ranga1; John Stephen Gushit4

منتشرة في المياه المهجورة من خلال الصوت على غشاء ركيزة نترات السليلوز تحت ضغط تفاضلي ثابت تم تمييز الأغشية المعدة باستخدام تقنيات مختلفةبما تم تحضير مستحلب الزيت/الماء لتقييم أداء فصل الغشاء عن طريق التحريك زيت .TGA و SEM و TEM و XRD و ATR-IR في ذلك في الماء مع كبريتات دوديسيل الصوديوم كمادة خافضة للتوتر السطحي حدد تشتت الضوء الديناميكي توزيع حجم القطرة للمستحلب. تم R-2 أولفاك تقييم أداء فصل الأغشية المركبة بناءً على رفض النفط التدفق، والخصائص المضادة تم حساب إجمالي انخفاض التدفق ونسبة استرداد التدفق لتقييم المقاومة أظهر الغشاء المركب مقاومة XRD مع بنية بلورية محتفظ بها أكدتها UiO-66-g-PEGMA الفاسدةأشارت النتائج إلى نجاح توليف وتطعيم المطعم المحبب للماء وفراغات بين الجسيمات مملوءة جزئياً، مما PEGMA إدخال UiO-66-NH2...ورفضًا معززين للقاذورات مقارنة بالبكر تحسنًا في تدفق المياه والقدرات المضادة للنفط دون المساس بالاحتفاظ UiO-66-g-PEGMA يساهم في تحسين أداء الترشيح أظهر الغشاء في تصميم أغشية عالية الأداء من أجل الفصل UiO-66-g-PEGMA بالنفطتسلط هذه الدراسة الضوء على الإمكانات الواعدة للأغشية المركبة الفعال بين النفط والماء. يوفر البحث رؤى قيمة حول تطبيق تقنيات التوليف غير العضوية في التصدي للتحديات المرتبطة بفصل المستحلب في عمليات الفصل بين النفط والماء

## Introduction

In the realm of inorganic synthesis and characterization, the study delves into the exploration of a UiO-66-g-PEGMA composite membrane for optimized oil/water emulsion separation performance. Oil/water emulsion mixtures, integral to various industrial processes, are classified into oil-in-water and water-in-oil emulsions based on the dispersion phase, their stability influenced by factors such as oil type, droplet size, and surfactant characteristics **(**Maria Teresa and Garcia Rubio, 2008; Yanqing, *et al*., 2017).

The global challenge of separating emulsified oil/water mixtures is underscored by the extensive production of oily wastewater in industrial operations (Xue, *et al.,* 2014; Chih-Feng, and Liang-Ting, 2017). The resulting environmental pollution from conventional disposal methods emphasizes the pressing need for effective technologies to treat such mixtures before discharge.

Investments in efficient technologies for treating oil/water mixtures have been driven by industrial adherence to environmental protection policies. However, conventional methods, including air flotation, gravity separation, settling tanks, and various chemical processes, often fall short due to high energy requirements, complex separation steps, and the generation of secondary pollutants (Zhang, *et al.,* 2018; Cheryan and Rajagopalan,1998).

Consequently, there is a growing demand for simple and economical separation approaches, particularly for complex mixtures like emulsified oil/water. Membrane technology emerges as a promising solution, offering advantages such as compact design, low energy consumption, high efficiency, and environmental friendliness (Zhu, *et al.,* 2014; Pham, *et al.,* 2011; Zahid, *et al.,* 2018)

Addressing challenges associated with oily wastewater, two types of oil/water separation membranes, namely oil-removing and water-removing membranes, have been employed. Common pressure-driven processes like microfiltration (MF), nano filtration (NF), ultrafiltration (UF), and reverse osmosis (RO) allow the passage of emulsified mixtures through a porous system while retaining oil on the membrane surface **(**Gebreslase, 2005**;** Cheng, *et al.,* 2017; Muppalla, *et al.*,2015).

However, these membrane processes face issues such as fouling due to intrinsic oleophilicity and the formation of a barrier layer by the denser water phase, hindering oil permeation (Ju, *et al.,* 2008; Miller, *et al.,* 2017).

To overcome these challenges, the study explores the surface modification of polymeric membranes by incorporating inorganic oxide nanoparticles like titanium dioxide ($TiO_2$), silicon dioxide ($SiO_2$), and zinc oxide (ZnO). While enhancing hydrophilicity and antifouling properties, these modifications encounter challenges such as agglomeration and unstable pore structures. Metal-organic frameworks (MOFs), exemplified by UiO-66-$NH_2$, present a potential solution with their unique nanochannels, high porosity, water stability, and tunable pore size Nady, *et al.,* 2011; Xiang, *et al.,* 2017; Maximous, *et al.,* 2009). UiO-66-$NH_2$, specifically, possesses water stability and functional groups that facilitate surface modification, preventing fouling.

This research focuses on the development of a novel oil/water emulsion nanocomposite membrane by grafting polyethylene glycol methacrylate (PEGMA) from the surface of UiO-66-$NH_2$. The synthesis process involves UiO-66-$NH_2$ nanoparticle preparation, grafting with hydrophilic PEGMA through atomic transfer radical polymerization (ATRP), and fabrication of composite membranes by nanoparticle deposition on cellulose nitrate substrate membranes. Evaluation of the fouling properties of both pristine and grafted composite membranes was conducted using a dead-end filtration setup, measuring parameters such as water flux, rejection ratio, flux recovery ratio (FRR), and flux decline ratio (DR). The incorporation of ethylene glycol dimethacrylate (EGDM) in the monomer for polymerization introduces cross-linking between nanoparticles and support, forming compact hydrated layers that prevent membrane fouling by oil droplets and facilitate easy cleaning (Bottino, *et al*., 2002; Valenzano, *et al.,* 2011).

## Materials and Method

Zirconium tetrachloride ($ZrCl_4$) (purity > 99.9%) and 2-amino-terephthalic acid (purity > 99%) were procured from Sigma-Aldrich. The N,N-Dimethylformamide (DMF), obtained from Wako Chemical Industries Ltd., served as the solvent for UiO-66-$NH_2$ nanoparticle preparation. A CN membrane (diameter: 47 mm, pore size: 0.1 μm, Whatman) was employed as the support membrane. Copper (I) chloride (CuCl), copper (II) chloride ($CuCl_2$), and 2,2'-bipyridine were acquired from Wako Chemical Industries Ltd. Lubricant Ulvac Oil R-2 (Sigma Aldrich) was used for nanoemulsion preparation. Sodium dodecyl sulfate (SDS), obtained from Kanto Chemical Co., Inc., was utilized as a surfactant. Deionized water was consistently used throughout the experiment.

### *Preparation of UiO-66-$NH_2$ Nanoparticles*

Under an inert atmosphere, a $ZrCl_4$ solution was prepared by reacting $ZrCl_4$ (1.63 mmol) and 2-amino-terephthalic acid (2.28 mmol) in 30 mL of DMF. Subsequently, 0.24 mL of deionized water was added to the reaction mixture, and the mixture was heated at 100 °C for 12 hours with constant stirring, resulting in a yellowish dispersion. The nanoparticles were collected by centrifugation and washed three times with 50 mL of DMF. The solid product was further washed with MeOH to completely remove DMF and then dried in a

Shangkum Yildun Goji1; Godwin Mafuyai2; Museyilnen Gocheka Mudel1; Jacob Shimwan Toekwal3; Rabiat Lawal Abdullahi1; Yusuf Garba Ranga1; John Stephen Gushit4

vacuum oven at 100 °C for 24 hours. The synthesis is detailed in Figure 1.

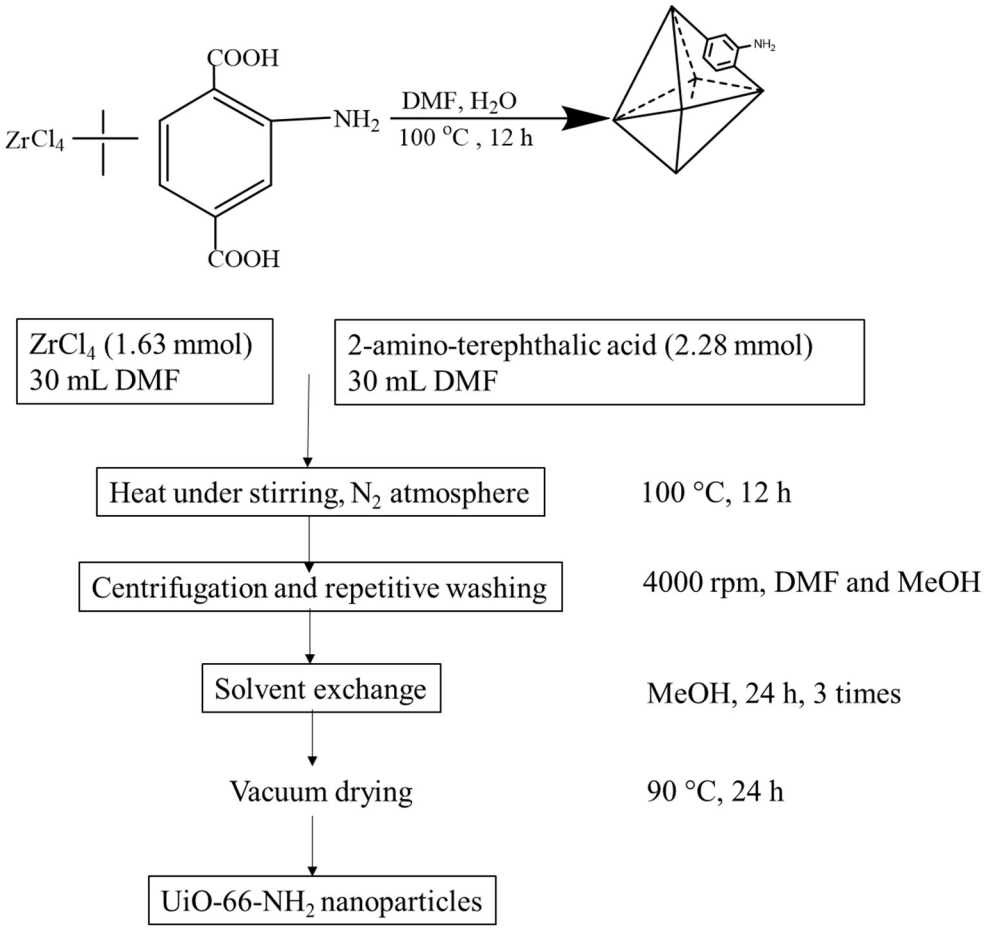


**Figure 1: Scheme for Synthesis of UiO-66-$NH_2$ Nanoparticles**

***Synthesis of UiO-66-g-PEGMA Nanoparticles for Enhanced Membrane Performance in Oil/Water Emulsion Separation***

UiO-66-g-PEGMA nanoparticles were synthesized using 2-bromopropionyl bromide (2-BPB) as the initiator. The initiator solution was prepared by dissolving 15 mmol of 2-BPB in 100 mL of tetrahydrofuran under a nitrogen atmosphere. EGDMA and a catalyst solution were prepared by dissolving 0.05 mol EGDMA in a 100 mL aqueous solution containing 0.3 mmol CuCl, 0.05 mmol $CuBr_2$, and 0.5 mmol 2,2'-bipyridyl. Ethylene glycol methacrylate was then polymerized from the grafted initiator in the presence of CuCl/$CuCl_2$/2,2'-bipyridine, followed by washing and storage in deionized water. The synthesis protocol for preparing UiO-66-g-PEGMA nanoparticles is illustrated in Figure 2.

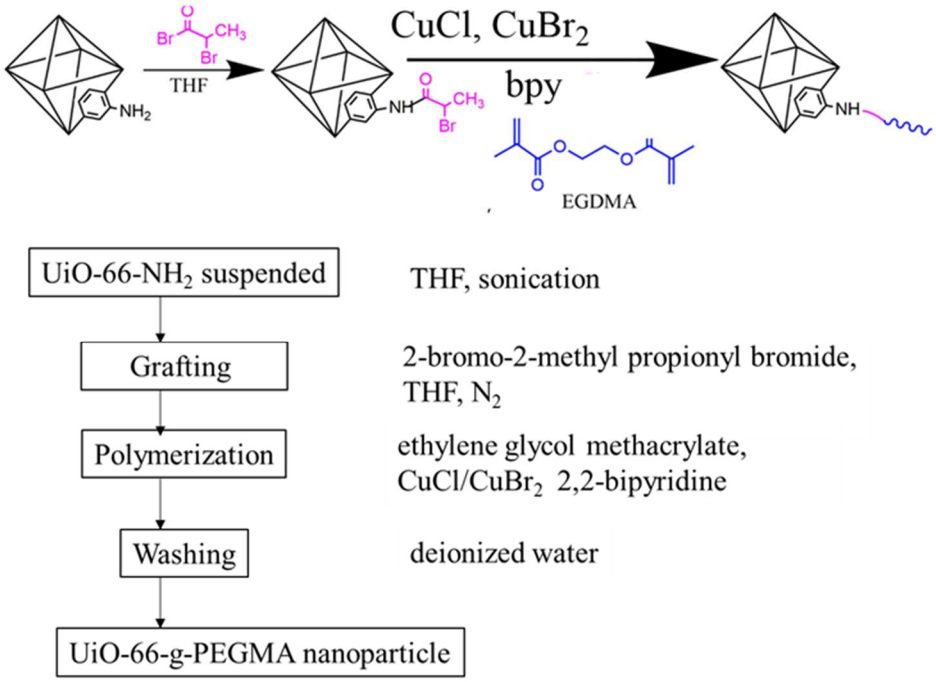


**Figure 2: Scheme for Synthesis of UiO-66-g-PEGMA Nanoparticles**

### *Fabrication of Composite Membranes*

Pristine UiO-66-$NH_2$ and UiO-66-g-PEGMA composite membranes were prepared through vacuum suction filtration. Each sample (2.4 mg) was dispersed in 30 mL of deionized water through sonication for 30 minutes. The dispersion was then deposited onto a cellulose nitrate (CN) substrate membrane via suction filtration, maintaining a constant differential pressure of 50 mbar. The substrate membrane was positioned on a filter glass holder and wetted with deionized water. After 30 minutes of filtration, the differential pressure was increased to 100 mbar and maintained for 15 minutes to partially dry the membrane. The pressure was sustained for an additional 30 minutes, and 100 mL of pure water was filtered through for compaction.

### *Oil/Water Emulsion Preparation*

The oil/water emulsion, utilized to evaluate the separation performance of the composite membranes, was created by adding 60 mg of Ulvac oil R-2 to 1.0 L of water in the presence of sodium dodecyl sulfate (SDS) as a surfactant. The mixture was stirred for 12 hours at 560 rpm, and the droplet size distribution of the oil/water emulsion was determined by dynamic light scattering (DLS) using a Nano Zetasizer from Malvern Instruments.

### *Characterization of Nanoparticles*

The attenuated total reflection infrared spectroscopy (ATR-IR) of the dried powder samples was conducted using a Jasco FT/IR-6100 spectrometer in the range of 400-4000 $cm^{-1}$ with a resolution of 4 $cm^{-1}$. X-ray diffraction (XRD) analysis of the crystalline structure of dried nanoparticles was performed using a Rigaku Smart Lab instrument with Cu $K_\alpha$ radiation ($\lambda$=1.54 Å),

Shangkum Yildun Goji1; Godwin Mafuyai2; Museyilnen Gocheka Mudel1; Jacob Shimwan Toekwal3; Rabiat Lawal Abdullahi1; Yusuf Garba Ranga1; John Stephen Gushit4

operating at 40 kV and 30 mA in the range of $5° \leq 2\theta \leq 40°$. The morphologies of UiO-66-$NH_2$ and UiO-66-g-PEGMA nanoparticles were observed using a transmission electron microscope (TEM, Hitachi H7100) at an accelerated voltage of 100 kV. The dried samples were dispersed in MeOH, deposited onto a copper grid by drop casting, and then air-dried. Particle size was determined through TEM image analysis using ImageJ software. Thermogravimetric analysis (TGA) of the samples was carried out on a Rigaku ThermoPlus EVO II thermal analyzer. The samples were loaded in an alumina pan and heated from room temperature to 800°C at a heating rate of 5°C/min under dry air.

### *Characterization of Composite Membranes*

The morphologies of the prepared composite membranes were examined using a scanning electron microscope (SEM, Hitachi S-4100) operating at an accelerated voltage of 20 kV. Prior to measurement, a sample piece was affixed to carbon tape and subjected to Pd/Pt sputtering for 100 s. Elemental analysis was performed using the energy-dispersive spectrometer TM3030-Plus model at an accelerated voltage of 15 kV.

### *Separation Performance of Composite Membranes*

The separation performance of the composite membranes was assessed based on oil rejection. The emulsion was poured onto the membrane, and water permeated at a constant differential pressure of 800 mbar. The concentrations of oil in the feed and permeate solutions were determined using UV/vis spectroscopy (Jasco V670) based on the absorption intensity at 280 nm. Permeate solutions were collected at intervals of 1, 2, 5, and 10 minutes, and the rejection (R) was calculated using Eq. (1):

$$R\ (\%) = \left(\frac{C_0 - C_p}{C_0}\right) \times 100 \qquad (1),$$

where concentrations ($C_0$) represent the feed and ($C_p$) the permeate. Flux was determined from the cumulative permeate volumes at specified filtration times using Eq. (2):

$$J = \left(\frac{V}{A \times t}\right) \qquad (2)$$

where J represents flux (L/m² h), V is the cumulative permeate volume, A is the effective area of the membrane (9.61 cm²), and t is the filtration time. The results were averaged over two separate experiments.

### *Total Flux Decline and Flux Recovery Ratio*

The ability of the prepared composite membranes to resist fouling was evaluated in terms of total flux decline (TR) and flux recovery ratio (FRR) of pristine UiO-66-$NH_2$ and UiO-66-g-PEGMA. The membranes were initially pre-compacted under 0.5 bar with deionized water to establish stable flux. Pure water flux ($J_{w1}$) was measured at 800 mbar for five minutes. Subsequently, a 10-minute filtration of oil/water emulsion was conducted, and the flux was recorded as $J_{w/o}$. The membrane was then washed with deionized water for approximately 60 minutes, followed by another 5-minute filtration of deionized water, and the recovered flux was recorded as $J_{w2}$. TR and FRR ratios were calculated to assess the antifouling properties of the membranes using the following equations:

$$TR = \left(1 - \frac{J_{w/o}}{J_{w1}}\right) \times 100\% \qquad (3),$$

$$FRR = \frac{J_{w2}}{J_{w1}} \times 100\% \qquad (4)$$

### *Fouling Analysis and Membrane Resistance Ratios*

To comprehensively analyze the fouling process, various ratios were formulated to characterize the fouling resistance of the prepared membrane. Additionally, reversible fouling ratio ($R_r$) and irreversible fouling ratio ($R_{ir}$) were defined and calculated using the following equations:

$$R_r = \frac{J_{W2} - J_P}{J_{W1}} \times 100\% \quad (5)$$

$$R_{ir} = \frac{J_{W1} - J_{W2}}{J_{W1}} \times 100\% \quad (6)$$

where $J_p$ (L/m² h) represents the permeate flux.

## Results and Discussion

### *Characterization of UiO-66-NH₂ and UiO-66-g-PEGMA Nanoparticles*

The successful synthesis of pristine UiO-66-$NH_2$, achieved through the addition of water as a modulator, and its subsequent grafting to produce UiO-66-g-PEGMA were confirmed through spectroscopy, specifically based on ATR-IR. As depicted in Figure 3a, the ATR-IR spectrum of pristine UiO-66-$NH_2$ displays a band at 485 $cm^{-1}$, corresponding to the newly formed Zr–O bond during MOF synthesis. Additional peaks include 846 $cm^{-1}$ for C-H rocking vibration, 1442 $cm^{-1}$ for primary amine, 1257 $cm^{-1}$ for C-N stretch vibration, and 1566 $cm^{-1}$ indicating interaction between –COOH and Zr (IV). Upon grafting, new absorption peaks at 1726 $cm^{-1}$ (carbonyl group vibration), 1098 $cm^{-1}$, and 946 $cm^{-1}$ (C-O-C and C-O stretching, respectively) emerge. The strong band at 2874 $cm^{-1}$ may be attributed to C–H stretching vibration for UiO-66-g-PEGMA. Notably, the absence of the stretching vibration peak at 1638 $cm^{-1}$ in the spectrum of UiO-66-g-PEGMA suggests complete polymerization of the monomer EGMA (Zhang, *et al*., 2018; Ong, *et al*., 2013; Roghani-Mamaqani, et al., 2014; Masuelli, *et al.,* 2012; Wandera, *et al.,*2011; Chen, *et al.,* 2009; Reddy, *et al.,* 2017; Cavka, *et al.,* 2008).

The XRD pattern (Figure 3b) for pristine UiO-66-$NH_2$ aligns consistently with the UiO-66 topology (Kandiah*, et al.,* 2010). Covalent attachment of the initiator onto UiO-66-$NH_2$ before UiO-66-g-PEGMA formation does not alter its crystal structure, as evidenced by an identical XRD pattern to pristine UiO-66-NH2. The diffraction pattern at 2-theta angles (7.26, 8.39, 11.93, and 14.64) corresponds to the (111), (002), (022), and (222) planes, confirming the preservation of MOF crystalline structure after polymerization (Wolavi, *et al.,* 2018; Kandiah, *et al.,* 2010). of Pristine UiO-66-$NH_2$ and UiO-66-g-PEGMA Nanoparticles

Shangkum Yildun Goji1; Godwin Mafuyai2; Museyilnen Gocheka Mudel1; Jacob Shimwan Toekwal3; Rabiat Lawal Abdullahi1; Yusuf Garba Ranga1; John Stephen Gushit4

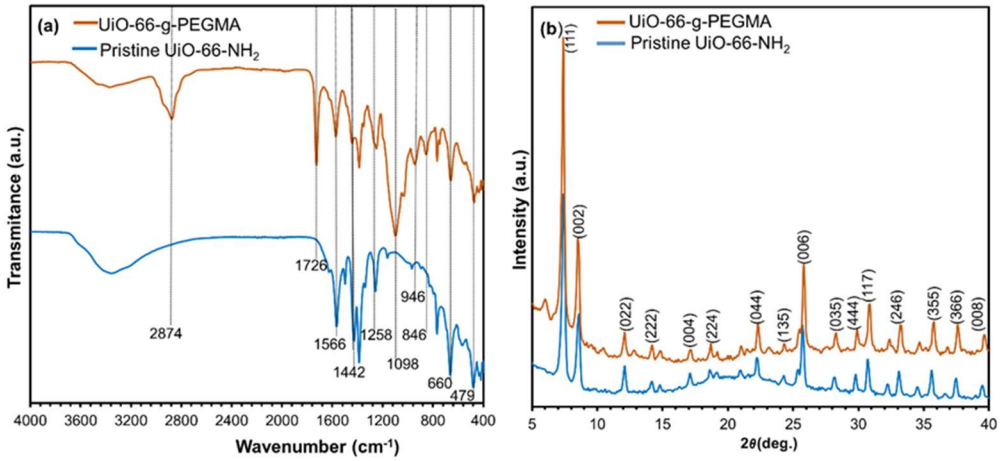


**Figure 3: a) Fourier Transform Infrared Spectra, and b) X-ray Diffraction Pattern**

Figure 2a is the TEM images of UiO-66-$NH_2$ and UiO-66-g-PEGMA nanoparticles that reveal symmetrical triangular base pyramids, maintaining similar morphologies (Sergio and Cohen, 2010). Notably, UiO-66-g-PEGMA crystals exhibit less-sharp edges and a rougher surface, indicative of the PEGMA polymer shell formation around the MOF nanoparticles. The particle sizes, estimated using ImageJ software, are 96 ±12 nm for UiO-66-$NH_2$ and 98± 09 nm for UiO-66-g-PEGMA (Figure 2b). This analysis underscores that the grafting process with PEGMA does not alter the pristine MOF morphology, emphasizing the stability of the MOF structure post-polymerization.

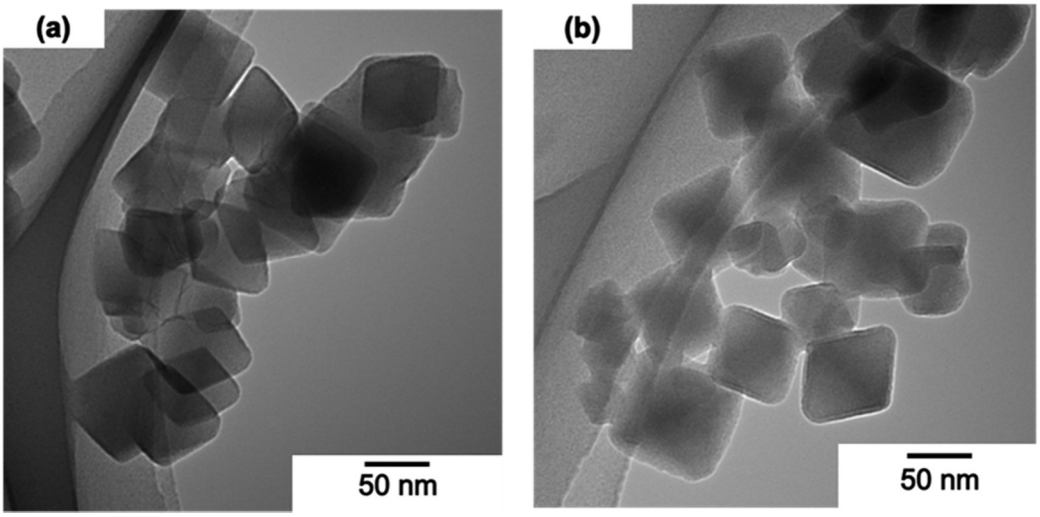


**Figure 3: TEM images depicting (a) pristine UiO-66-$NH_2$ and (b) UiO-66-g-PEGMA nanoparticles**

The Figure 4 is the nanocomposite membrane morphology and elemental distribution within the matrix of the nanocomposite membranes. In Figure 4a is SEM image of the pristine UiO-66-$NH_2$ nanocomposite membrane that revealed a partial distribution of nanoparticles on the substrate membranes, leading to the generation of interparticle voids while Figure b is EDS mapping scanning spectrum that displays a uniform distribution of zirconium atoms on the composite membrane surface which are indicated by the red coloration signal. Figures c, d, e) are the EDS spectra that illustrate the elemental distribution of Zr, O, and C in the pristine UiO-66-$NH_2$ composite membrane and f) SEM image of UiO-66-g-PEGMA composite membrane shows grafted nanoparticles uniformly distributed and interconnected, minimizing interparticle voids compared to Figure 4a. The Figure 4g EDX image reveals a quantitative decrease in the red signal (zirconium content) compared to the pristine composite membrane. The Figures 4h, 4i, 4j are the individual elemental content for Zr, O, and C. These observations suggest complete polymerization of the monomer on the nanoparticle surface, contributing to enhanced membrane structure.

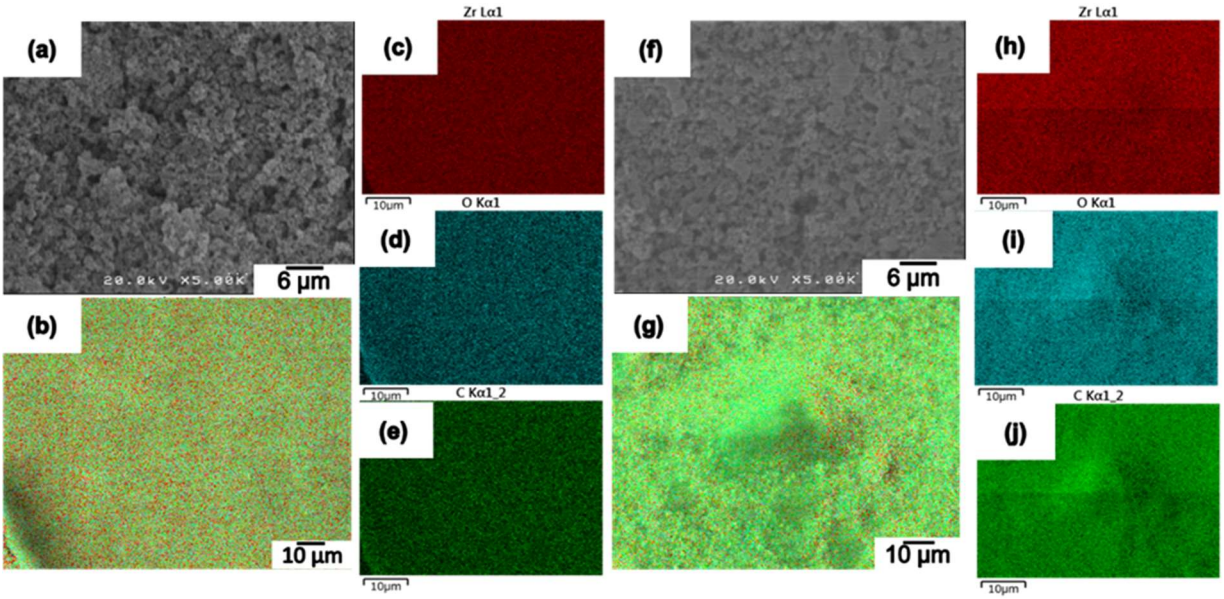


**Figure 4: Top View SEM-EDX Images of Composite Membranes: a, b, c, d, e) Top view SEM-EDX images of pristine UiO-66-$NH_2$ nanocomposite membrane, f, g, h, i, j) Top view SEM-EDX images of UiO-66-g-PEGMA composite membrane.**

***Thermal Stability Analysis of UiO-66-$NH_2$ and UiO-66-g-PEGMA Nanoparticles via Thermogravimetric Analysis (TGA)***

The thermal stabilities of UiO-66-$NH_2$ and UiO-66-g-PEGMA were investigated using thermogravimetric analysis (TGA) in an air atmosphere, and the corresponding thermograms are presented in Figure 5. The TGA curves exhibit a two-step weight loss pattern. The initial weight loss, occurring at 190 °C, is attributed to the vaporization of adsorbed water molecules within the porosity of the nanoparticles and the loss of residual monomer. The subsequent weight loss,

observed around 354°C, is associated with the decomposition of the frameworks (Cao, *et al.,* 2018; Sergio and Cohen, 2010). Comparing the weight loss profiles between UiO-66-$NH_2$ and UiO-66-g-PEGMA, differences are evident in the TGA curves, confirming the successful grafting of PEGMA onto UiO-66-NH2 via ATRP. The thermograms indicate that the percentage of inorganic residues for pristine UiO-66-$NH_2$ and UiO-66-g-PEGMA is estimated at 24% and 29%, respectively, as displayed on the thermograms.

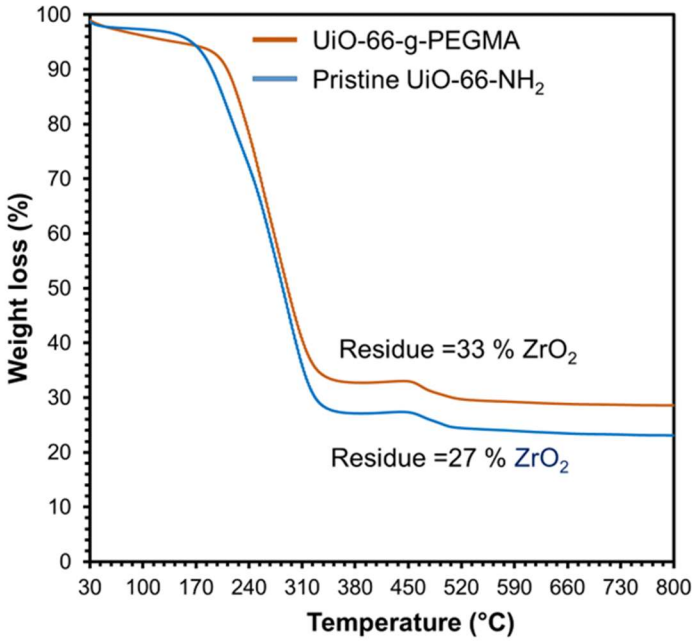


**Figure 5: Thermogravimetric Analysis (TGA) Profile of Pristine UiO-66-$NH_2$ and UiO-66-g-PEGMA Nanoparticles**

### *Separation Performance of UiO-66-$NH_2$ and UiO-66-g-PEGMA Composite Membranes*

Figure 6a illustrates the separation performance of the composite membranes and evaluated based on the rejection of oil/water emulsion. The oil rejection percentages for pristine UiO-66-$NH_2$ and UiO-66-g-PEGMA composite membranes were 89.6% and 96.4%, respectively, at a dosage of 2.4 mg. The high permeability flux with lower oil rejection observed in the case of the pristine UiO-66-$NH_2$ composite membrane may be attributed to interparticle voids. The grafting and polymerization processes involved in producing the UiO-66-g-PEGMA composite membrane led to higher rejection for the oil/water emulsion, thanks to increased hydrophilicity resulting from grafting EGMA onto the nanoparticle surfaces. This process narrowed the interparticle voids, resulting in lower permeability.

The flux decline for both composites is depicted in Figure 6b. The results indicate that UiO-66-g-PEGMA exhibited significant resistance to flux decline, as evidenced by the steadiness of the curves compared to the rapid

decline observed in the pristine UiO-66-$NH_2$ composite membrane. This suggests that grafting significantly enhances rejection by reducing the propensity of the composite membrane to fouling through the adhesion of oil to the membrane surface.

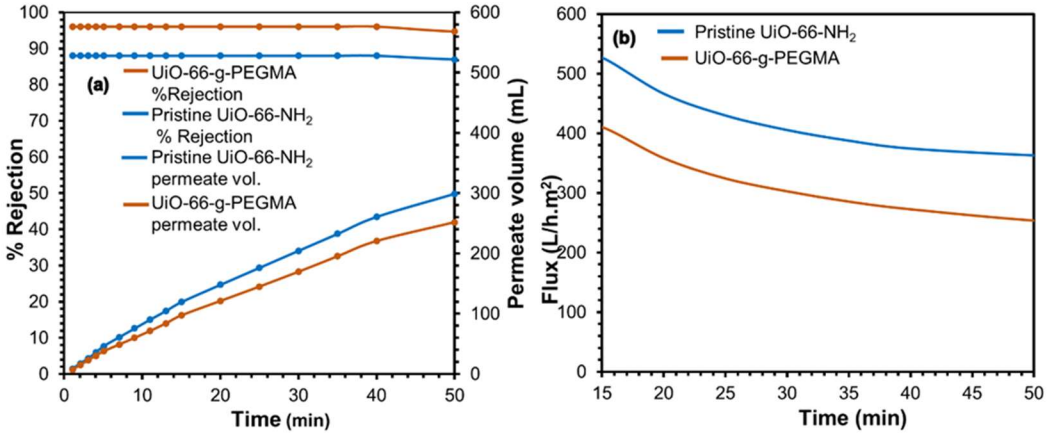


**Figure 6: Separation Performance of a) Pristine UiO-66-$NH_2$ and UiO-66-g-PEGMA at 3.6 mg Loading b) Total Flux Decline Ratio.**

Figure 7, the characteristics of the oil/water emulsion size, determined through dynamic light scattering (DLS), are presented. DLS is a technique commonly employed to analyze particle size distributions in colloidal systems. The emulsion size is depicted as a function of intensity (percent), indicating the relative abundance of droplets at different sizes. The graph illustrates that the droplet size of the oil/water emulsion is predominantly around 100 nm. This signifies that a substantial portion of the emulsion consists of droplets with diameters close to this specific size. The intensity (percent) on the y-axis represents the distribution of droplet sizes in the emulsion, with 100 nm being the prevalent size. Understanding the size distribution of the emulsion is crucial for evaluating its stability and interaction with separation membranes. In the context of oil/water separation, the emulsion's size can influence factors such as permeation through membranes, fouling tendencies, and overall separation efficiency. Therefore, the presented DLS analysis offers valuable insights into the physical characteristics of the oil/water emulsion under investigation

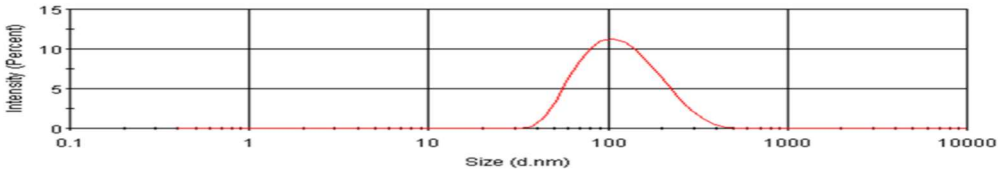


.

**Figure 7: Size distribution of an oil-water emulsion prepared with SDS as the surfactant, as measured using Dynamic Light Scattering (DLS).**

Shangkum Yildun Goji1; Godwin Mafuyai2; Museyilnen Gocheka Mudel1; Jacob Shimwan Toekwal3; Rabiat Lawal Abdullahi1; Yusuf Garba Ranga1; John Stephen Gushit4

### Impact of Loading on the Antifouling Properties of Pristine UiO-66-$NH_2$ and UiO-66-g-PEGMA Nanoparticles

To comprehensively understand the influence of loading of pristine UiO-66-$NH_2$ and UiO-66-g-PEGMA nanoparticles on the performance of composite membranes, the nanoparticle contents were varied within the range of 0.6 mg to 4.0 mg, as illustrated in Figure 8. Both composite membranes exhibited a notable increase in oil droplet rejection with the rise in nanoparticle loading. However, the UiO-66-g-PEGMA composite demonstrated significantly higher oil rejection compared to the pristine composite membrane. This enhancement can be attributed to the increased hydrophilic groups in UiO-66-g-PEGMA, originating from PEGMA. Consequently, the addition of UiO-66-g-PEGMA improved the hydrophilicity of the membrane, facilitating the passage of water molecules through the membrane (Tan, *et al.,* 2018; Ibrahim, *et al*., 2019).

The flux decline ratios, expressed as percentages, are depicted in Figure 6b. The TR, FRR concerning % flux showed perfect parabolic curves in the case of UiO-66-g-PEGMA, unlike the pristine UiO-66-$NH_2$, which displayed a declining linear relationship (Sastre, et al., 1988). Moreover, membranes with higher FRR values and lower TR values suggest that foulants encounter difficulties in being adsorbed on the surface and can be easily washed away. The calculated values of flux, (Rr), and (Rir) ratios are tabulated in Table 1.

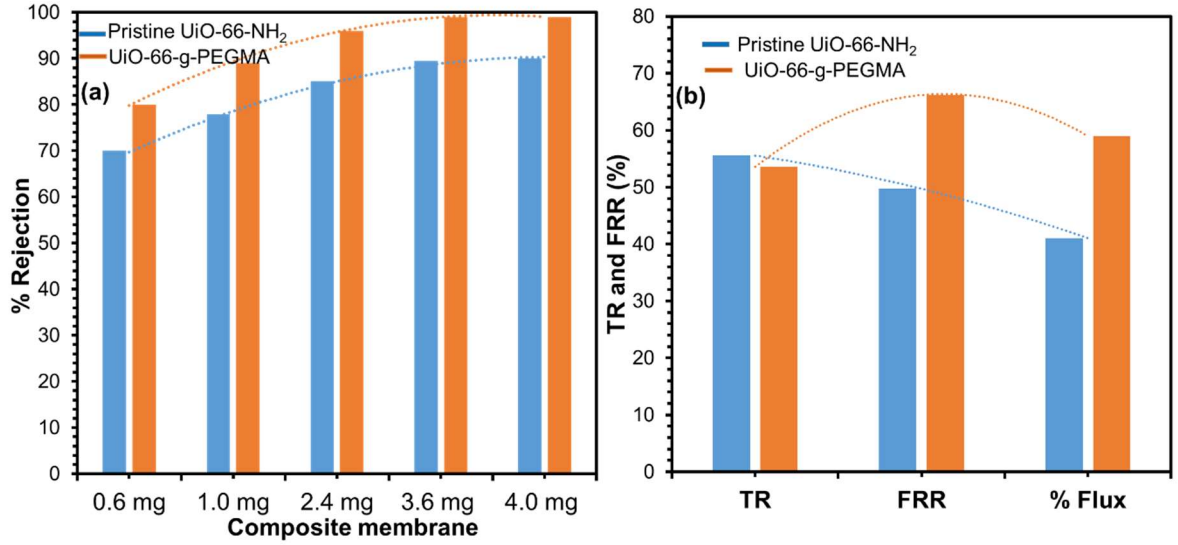


**Figure 8: Illustrates the percentage of oil/water emulsion rejection by composite membranes, showcasing a) the performance of Pristine UiO-66-$NH_2$ and UiO-66-g-PEGMA at various loadings, and b) the total flux decline ratio (TR) and flux recovery ratio (FRR) for Pristine UiO-66-$NH_2$ and UiO-66-g-PEGMA membranes loaded at 3.6 mg.**

### *A Comparative Analysis of Flux Recovery, Reversible Fouling, and Irreversible Fouling in UiO-66-$NH_2$ and UiO-66-g-PEGMA Membranes*

To gain deeper insights into the antifouling performance, the flux recovery ratio (FRR), reversible fouling ratio (Rr), and irreversible fouling ratio (Rir) were calculated using equations (3)-(6) based on the first cycle separation of membrane fouling and washing. The results are presented in Table 1. For pristine UiO-66-$NH_2$, a TR of 55.56% was obtained, decreasing to 49.72% for its FRR. In contrast, UiO-66-g-PEGMA exhibited an increase in FRR from 53.56% to 66.18%. Additionally, pristine UiO-66-$NH_2$ showed a low percentage of reversible fouling (19.50%) and a high value for irreversible fouling (50.24%), while UiO-66-g-PEGMA displayed higher percentage values for reversible (32.03%) and irreversible fouling (45.04%). Higher FRR values generally indicate better antifouling properties of the composite membrane. The enhanced antifouling properties of UiO-66-g-PEGMA membrane can be attributed to the increased hydrophilicity resulting from grafting, demonstrating its superior antifouling performance.

**Table 1: Flux and antifouling parameters of composite membranes**

| Composite membrane | TR (%) | FRR (%) | $R_r$ (%) | $R_{ir}$ (%) | Flux (%) | Flux ($L/m^2.h$) |
|---|---|---|---|---|---|---|
| Pristine UiO-66-$NH_2$ | 55.56 | 49.72 | 19.50 | 50.24 | 41.04 | 513±09 |
| UiO-66-g-PEGMA | 53.56 | 66.18 | 32.03 | 45.04 | 58.98 | 737±11 |

[a]Total flux decline (TR), [b]Flux recovery ratio (FRR) [c]Reversible fouling ratio ($R_r$), [d]Irreversible fouling ratio ($R_{ir}$) were calculated according to Eq.(3)-(6) respectively.

## Conclusion

In conclusion, our exploration into the synthesis and characterization of UiO-66-g-PEGMA composite membranes has yielded a novel solution for achieving highly efficient oil/water emulsion separation. Through the innovative deposition method, UiO-66-$NH_2$ nanoparticles were first subjected to ATRP to graft PEGMA, and the resulting UiO-66-g-PEGMA membrane was fabricated through suction filtration on a CN substrate. XRD analysis confirmed the retention of the crystalline structure in UiO-66-$NH_2$, indicating the successful polymerization of PEGMA. The composite membrane exhibited increased fouling resistance and rejection rates compared to pristine UiO-66-$NH_2$ nanoparticles.

The introduction of grafted PEGMA not only enhanced the hydrophilicity of the composite membrane but also contributed to the partial filling of interparticle voids. The filtration performance of the UiO-66-g-PEGMA composite membrane was notably improved, and this enhancement was attributed to the increased amount of grafted PEGMA. Importantly, the novel membrane demonstrated significantly improved water flux and antifouling capabilities without compromising oil retention.

This research underscores the promising potential of UiO-66-g-PEGMA in the design of composite membranes tailored for effective oil/water separation. The fabricated membrane represents a significant advancement in addressing the challenges associated with emulsion separation, emphasizing the practical application of inorganic synthesis techniques for the development of high-performance membranes in oil-water separation processes.

**References**

**Adham, S.; Hussain, A.; Minier-Matar, J.; Janson, A.; Sharma, R (2018).** Membrane applications and opportunities for water management in the oil & gas industry. *Desalination* 440, 2−17

**Ahmed, N. A.; Goh, P. S.; Karim, Z. A.; Ismail, A. F (2018).** Thin film composite membrane for oily wastewater treatment: recent advances and challenges. *Membranes*, 8, 86.

**Al-Shamrania, A. A.; Jamesa, A.; Xiao, H (2002).** Destabilisation of oil–water emulsions and separation by dissolved air flotation*Water Resour*. 36, 1503–1512.

**Bottino, A.; Capanelli, G.; Comite, A (2002).** Preparation and characterization of novel porous PVDF-$ZrO_2$composite membranes. *Desalination* 146, 3540.

**Cao, Sergio and Cohen, (2010).** Self-assembled MOF membranes with under water superoleophobicity for oil/water separation. *J. Membr. Sc* 566, 268‑277.

**Cavka, (2008)**. A New zirconium inorganic building brick forming metal organic frameworks with exceptional stability. *J. Am. Chem. Soc.* 130. 13850‑13851.

**Chen, (2009)**. The improved oil/water separation performance of cellulose acetate-graft-polyacrylonitrile membranes. *J Membr. Sci* 337: 98-105.

**Cheng, Q.; Ye, D.; Chang, C.; Zhang, L (2017).** Facile fabrication of superhydrophilic membranes consisted of fibrous tunicate cellulose nanocrystals for highly efficient oil/water separation. *J. Membr. Sci.* 525, 1–8.

**Cheryan, M.; Rajagopalan, N (1998).** Membrane processing of oily streams: wastewater treatment and waste reduction. *J. Membr. Sci.*151, 13–28.

**Chih-Feng, W.; Liang-Ting, C (2017).** Preparation of super wetting porous materials for ultrafast separation of water-in-oil emulsions. *Langmuir* 44, 1969−1976.

**Gebreslase, A. G (2005).** Review on membranes for the filtration of aqueous based Solution: Oil in Water Emulsion. *J Membr Sci.Technol*. 2018, 8:2

**Ibrahim, (2019).** Carbon-based nanocomposite membranes for water and wastewater purifcation: Micro and Nano Technologies. In Advanced Nanomaterials for Membrane Synthesis and its Applications. 367, 23–44.

**Ju, H.; McCloskey, B. D.; Sagle, A. C.; Wu, Y. H.; Kusuma, V.A.; Freeman, B. D (2008).** Cross-linked poly (ethylene oxide) fouling resistant coating materials for oil/water

separation, *J. Membr. Sci.* 307, 260–267.

**Kandiah, M.; Usseglio, S.; Svelle, S.; Olsbye, U.; Lillerud, K. P.; Tilset, M (2010).** Post synthetic modification of the metal‑organic framework compound UiO-66. *J. Mater. Chem*. 20, 9848‑9851.

**Maria-Teresa, C.; Garcia-Rubio, L. H (2008).** Characterization of emulsions: A systematic spectroscopy study. *Journal of Dispersion Science and Technology*, 29:1, 20-26.

**Masuelli, (2012).** Preparation, structural and functional characterization of modified porous PVDF membranes by γ-irradiation. *J Membr. Sci* 389: 89, 91-98.

**Maximous, N.; Nakhla, G.; Wan, W.; Wong, K(2009).** Preparation, characterization and performance of $Al_2O_3$/PES membrane for wastewater filtration. *J. Membr. Sci*. 341, 67−75.

**Miller D. J.; Dreyer D. R.; Bielawski C. W.; Paul D. R.; Freeman B. D (2017).** Surface modification of water purification membranes. *Angew Chemie Int. Ed 56*: 4662−4711.

**Mohammad A. J. M.; Panchami H. R.; Arun M. I.; Muhammad, U.; Shakhawat H. C.; Shaikh A. A; Inamuddin A. A . A , (2020).** Assessment of sulfonated homo and co-polyimides incorporated polysulfone ultrafltration blend membranes for effective removal of heavy metals and proteins. *Scientific Reports* 10:7049, 1–13.

**Muppalla, R.; Jewrajka, S. K.; Reddy, A. V. R (2015).** Fouling resistant nanofiltration membranes for the separation of oil–water emulsion and micropollutants from water. *Sep. Purif. Technol*. 143, 125–134.

**Nady, N.; Franssen, M.C.R.; Zuilhof, H.; Eldin, M. S. M.; Boom R (2011).** Modification methods for poly (arylsulfone) membranes: A mini-review focusing on surface modification. *Desalination* 275, 1−9

**Padaki, M.; Murali. S. R.; Abdullah, M.S.; Misdan, N.; Moslehyani, A.; Kassim, M. A.; Hilal, N.; Ismail, A. F (2015).** Membrane technology enhancement in oil-water separation. A review. *Desalination* 357, 197−207

**Pham, T. C. T.; Kim, H. S.; Yoon, K. B (2011).** Growth of uniformly oriented silica MFI and BEA zeolite films on substrates. *Science* 334, 1533−1538.

**Reddy, (2017).** Polyethylene glycol methacrylate- grafted dicationic imidazolium-based ionic liquid: heterogeneous catalyst for the synthesis of aryl- benzo [4, 5] imidazole[1, 2] pyrimidine amines under solvent-free conditions. *Tetrahedron* 73, 5289-5292.

**Roghani-Mamaqani, (2014).** *In-situ* atom transfer radical polymerization of styrene to in plane functionalize graphene nanolayers: grafting through hydroxyl groups. *J. Polym. Res*. 21, 333−343.

**Sastre, et al. (1988).** Improved Techniques in Liquid Membrane Separations: An Overview. *Sep. Purif. Methods.* 27(2), 213–298.

**Sergio and Cohen, (2010).** Isoreticular synthesis and modification of frameworks with the UiO-66 topology. *Chem. Communication* 46, 7700‑7702.

**Tan, (2018)** Superhydrophilic and underwater superoleophobic poly (acrylonitrile-co-methyl acrylate) membrane for highly efficient separation of oil-in-water emulsions. *J. Membr. Sci*. 564, 712–72.

**Valenzano, L.; Civalleri, B.; Chavan, S.; Bordiga, S. Nilsen, M. H.; Jakobsen, S. Lillerud, K. P.; Lamberti, C (2011).** Disclosing the complex structure of UiO-66 metal organic framework: A synergic

combination of experiment and theory. *Chem. Mater*.23, 1700‑1718.

**Wandera, (2011).** Modification and characterization of ultrafiltration membranes for treatment of produced water. J Membr. Sci 373: 178-188.

**Wolavi, H.; Shojaei, A.; Mousavi, S. A (2018)**. Improving mixed-matrix membrane performance via PMMA grafting from functionalized $NH_2$-UiO-66. *J. Mater. Chem. A*. 6, 2775-2791.

**Xiang, S.; Tiande, X.; Jiangang, W.; Peng, L.; Fan, W (2017).** An anti-fouling poly (vinylidene fluoride) hybrid membrane blended with functionalized $ZrO_2$ nanoparticles for efficient oil/water separation. *RSC Adv.*7, 5262.

**Xue, Z.; Cao, Y.; Liu, N.; Feng, L.; Jiang, L (2014)**. J. Special wettable materials for oil/water separation Special wettable materials for oil/water separation. *Mater. Chem. A*. 2, 2445 - 2460.

**Yanqing, D.; Yujiang, L, Tao, W (2017).** A superhydrophilic and underwater superoleophobic chitosan–$TiO_2$ composite membrane for fast oil-in-water emulsion separation. *RSC Adv,* 7, 41838 –41846.

**Zahid, M.; Rashid, A.; Akram, S.; Rehan, Z. A.; Razzaq, W (2018).** A comprehensive review on polymeric nano-composite membranes for water treatment. *J. Membr Sci. Technol.* 8, 1−20.

**Zhang, (2018).** A facile method to prepare dual-functional membrane for efficient oil removal and in situ reversible mercury ions adsorption from wastewater. *Appl. Surf. Sci.* 434: 88, 57-62.

**Zhang, J.; Pan, X.; Xue, Q.; He, D.; Zhu L, ,(2017).** Antifouling hydrolyzed polyacrylonitrile/graphene oxide membrane with spindle-knotted structure for highly effective separation of oil-water emulsion. *J Membr. Sci* 532: 38-46.

**Zhang, X.; Zhao, Y.; Mu, S.; Jiang, C.; Song, M.; Fang, Q.; Xue, M.; Qiu, S.; Chen, B (2018).** UiO-66-coated mesh membrane with underwater superoleophobicity for high-efficiency oil−water separation. *ACS Appl. Mater. Interfaces* 10, 17301−17308.

**Zhu. Y.; Wang, D.; Jiang, L; Jin, J (2014).** Recent progress in developing advanced membranes for emulsified oil/water separation. *NPG Asia Materials* 6, e101.